Electronic Supplementary Information (ESI) for

Intrinsically stretchable sheath-core ionic sensory fibers with well-regulated conformal and reprogrammable buckling

Chenglong He, Shengtong Sun*, and Peiyi Wu*

E-mail: shengtongsun@dhu.edu.cn; wupeiyi@dhu.edu.cn

This material includes

Table S3 Comparison of the maximum strain and gauge factor of the buckled sheath-core fiber in this work with several other reported ionic sensors

References S1-S15

Movie S1. Fabrication of buckled sheath-core ionic sensory fiber
Movie S2. Stretching-induced reversible transparency of buckled fiber
Movie S3. Water droplet motion control on programmed buckled fibers
Movie S4. Comparison of the strain sensitivities of smooth and buckled fibers

Experimental

Materials. 2-Methoxyethyl acrylate (MEA), poly(ethylene glycol) diacrylate (PEGDA, M_n ~ 250 g/mol), and 2-(methacryloyloxy)ethyl]trimethylammonium chloride solution (MTMA Cl, 75 wt% in H_2O) were purchased from Sigma-Aldrich. Tetrahydrofuran (THF), bis(trifluoromethane)sulfonimide lithium salt (LiTFSI), and 2,2-diethoxyacetophenone (DEAP) were purchased from TCI Chemical (Shanghai). 1-Ethyl-3-methylimidazolium bis(trifluoromethylsulfonyl)imide (EMI TFSI) was purchased from Aladdin Reagent (Shanghai). Methyl isobutyl ketone (MIBK) was purchased from Sinopharm Chemical, China. Fluoroelastomer (PVDF-HFP-TFE terpolymer, containing 48 wt% PVDF, 19 wt%, HFP, 33 wt% TFE; glass transition temperature (T_g) ~ -26 ^oC) was purchased from Qingheng Plastic Raw Materials. MEA and PEGDA were purified with alumina to remove inhibitor and other reagents were used as received.

Synthesis of 2-(methacryloyloxy)ethyl]trimethylammonium bis(trifluoromethanesulfonyl)amide (MTMA TFSI). The preparation of MTMA TFSI was the same as previously reported.[S1] Briefly, the aqueous solutions of MTMA Cl and LiTFSI were mixed at a molar ratio of 1:1.2 to ensure the full reaction. An appropriate amount of deionized water was added to further dissolve the reactants, and the reaction was stirred at room temperature for 4 h. Subsequently, the reaction mixture was washed five times with water in a separate funnel to remove LiCl and unreacted residue. The resulting oily viscous liquid was vacuum dried at 60 ^oC for 10 h to obtain colorless MTMA TFSI for storage.

Preparation of P(MEA-co-MTMA TFSI) ionogel precursor. The optimal ionogel precursor (Entry 4 in Table S1) was prepared by mixing 1.012 g of MEA, 0.188 g of MTMA TFSI, 0.3365 g of EMI TFSI (final concentration = 0.64 M), 0.00245 g of crosslinker PEGDA (0.12 mol% of monomer), and 0.0017 g of photoinitiator DEAP (0.1 mol% of monomer). The above mixture was stirred and mixed with a centrifuge for 10 min, and then ultrasonicated for 10 min to remove bubbles before use.

Fabrication of P(MEA-co-MTMA TFSI) ionogel fiber. The above ionogel precursor was injected into a PTFE circular tube by a syringe and UV cured for 10 min. Subsequently, the P(MEA-*co*-MTMA TFSI) ionogel fiber was extracted nondestructively out of the PTFE tube. Different sizes of ionogel fibers can be prepared by adjusting the inner diameters of PTFE tube molds. Here, ionogel fibers with diameters of 400, 500, and 600 μm were prepared, respectively.

Preparation of fluoroelastomer solution with and without PEGDA. For the preparation of fluoroelastomer sheath with a typical thickness of 18 μm, 2 g of PVDF-HFP-TFE, PEGDA (6 wt%) and DEAP (4 wt%) were added into 30 mL of MIBK. For fluoroelastomer solution without PEGDA, only 2 g of PVDF-HFP-TFE was dissolved in MIBK (30 mL). For the sheath thicknesses of 10 and 40 μm, 1 g and 3 g of fluoroelastomer were dissolved in 30 mL of MIBK, respectively. The above solutions were stirred for 12 h to obtain uniform precursors for subsequent dip-coating.

Fabrication of sheath-core ionic sensory fiber. The sheath-core ionic sensory fiber with good uniformity was prepared by a dip-coating method. The P(MEA-*co*-MTMA TFSI) ionogel fiber was used as the core material. For sheath coating, the core-only fiber was dipped into the fluoroelastomer solution with PEGDA within 5 s and then vertically suspended for natural leveling in a dried desiccator. Finally, the smooth sheath-core fiber was obtained after being UV cured for 10 min to build strong adhesion between core and sheath. In the controlling fluoroelastomer coating without PEGDA, all the operations were the same except for the different fluoroelastomer solution and the last curing step was also not needed.

Fabrication of conformal buckling. The sheath-core ionic sensory fiber was stretched to a specified strain and held for 5 minutes in the vertical direction and then released to form a conformal buckling structure. The conformal buckles with different morphologies can be obtained by different loadings to control different holding strains.

Sensing with different calligraphy brushes. The smooth fiber and buckled fiber (produced at 500% holding strain) were fixed closely on a glass plate, which were respectively connected with platinum wires to a multichannel multimeter for detecting resistance changes. The diameter of the fiber is about 0.5 mm, and the effective contact length is about 3 cm, which ensures that the brush would cover it completely. The brush was controlled to smoothly rub the fibers back and forth, while a series of signals were obtained with the multimeter.

String plucking-like sensing. The smooth and buckled fibers (produced at 500% holding strain) were fixed on a vernier caliper close to each other. The effective test length is about 2.5 cm. A glass rod was used to pluck the two fibers in the same amplitude and at the same time to simulate the finger-plucking actions of musical instrument while the resistance signals were real-time recorded.

Perturbation correlation moving window (PCMW). FTIR spectra recorded with an increment of 2 ^{o}C during heating were employed to perform PCMW analysis. According to the method provided by Morita,[S2] the raw data were processed. Further correlation information was calculated by the software 2D Shige, ver. 1.3 (©Shigeaki Morita, Kwansei Gakuin University, Japan, 2004–2005) with an appropriate window size (2m + 1 = 11) to generate good quality PCMW spectra. Finally, the contour maps were plotted using Origin program, ver. 2021, with red colors indicating positive intensities while blue colors the negative ones.

Characterizations. The molecular weight and polydispersity of the used fluoroelastomer were determined by gel permeation chromatography (GPC, Shodex KD 803) with THF as the eluent. The morphological images of sheath-core fibers were taken using both scanning electron microscope (SEM, JSM-IT300, JEOL) and ultra-depth three-dimensional microscope (VHX-6000, Keyence). General tensile tests at the speed of 15 mm/min, loading-unloading cycling tests and peeling curves at the speed of 50 mm/min were collected on a vertical dynamometer (ESM303, MARK-10) at room temperature. Thermal gravimetric analysis (TGA) was performed on TA TGA550 under N_2 atmosphere from 25 to 700 ^{o}C at a heating rate of 10 ^{o}C/min. Differential scanning calorimetry (DSC) was performed on TA DSC250 at a temperature ramp of 10 °C/min from -80 to 200 °C under N_2 atmosphere. The transmittance of ionogel and fluoroelastomer was recorded on a UV–VIS–NIR spectrometer (Lambda 950, PerkinElmer). ATR-FTIR spectra and temperature-dependent ATR-FTIR spectra were recorded on a spectrometer (Nicolet iS50, Thermo Scientific) with diamond crystal as the window material. Tensile tests at specific temperatures were carried out on a dynamic thermomechanical analyzer (DMA, Q800, TA). The apparent static contact angle was measured on the contact angle analyzer (JD-901, JingDing). The platinum wires were used to connect the fibers to a multimeter (DMM 4050, Tektronix) or multi-channel multimeter (DAQ6510, Keithley) for resistance monitoring.

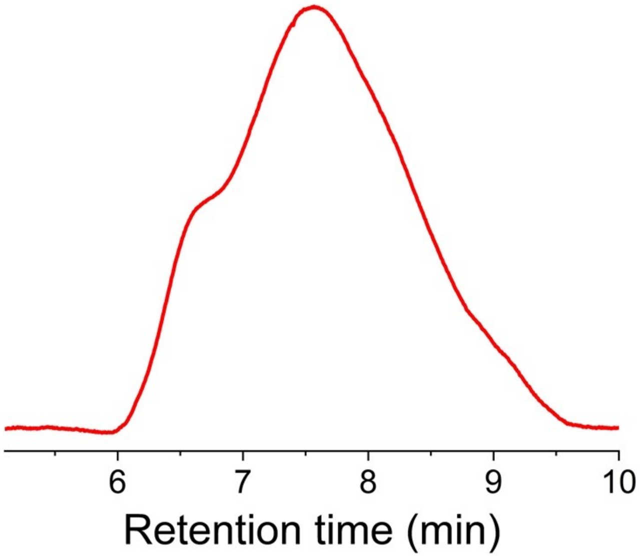

Fig. S1 GPC profile of the used PVDF-HFP-TFE fluoroelastomer. As calculated, the weight-average molecular weight (M_w) is 8.1×10^5 g/mol and polydispersity is 1.14.

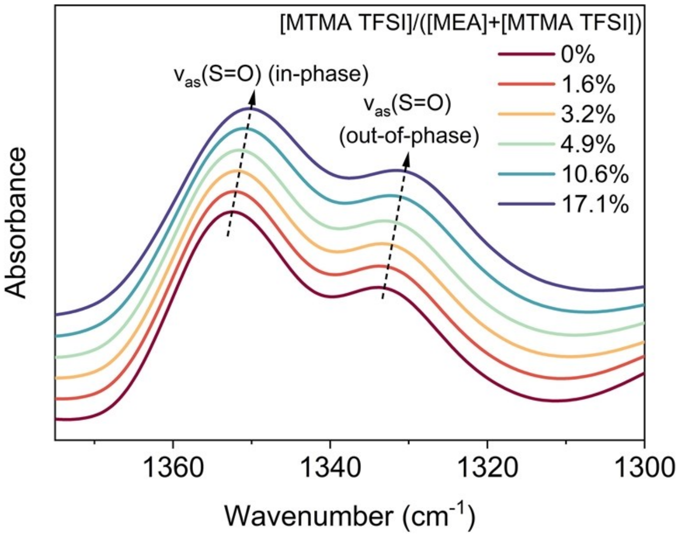

Fig. S2 ATR-FTIR spectra of P(MEA-*co*-MTMA TFSI) ionogels in the S=O (from TFSI) stretching region with different amounts of MTMA TFSI. With increasing MTMA TFSI content, both the in-phase and out-of-phase asymmetric S=O stretching vibrations around 1352 and 1333 cm^{-1} shift to lower wavenumbers, suggesting that the TFSI anions are more associated with EMI cations with a blocked mobility. For comparison, in pure IL with strongly associated ion pairs, v_{as}(S=O) (in-phase) = 1347 cm^{-1}, and v_{as}(S=O) (out-of-phase) = 1330 cm^{-1}.

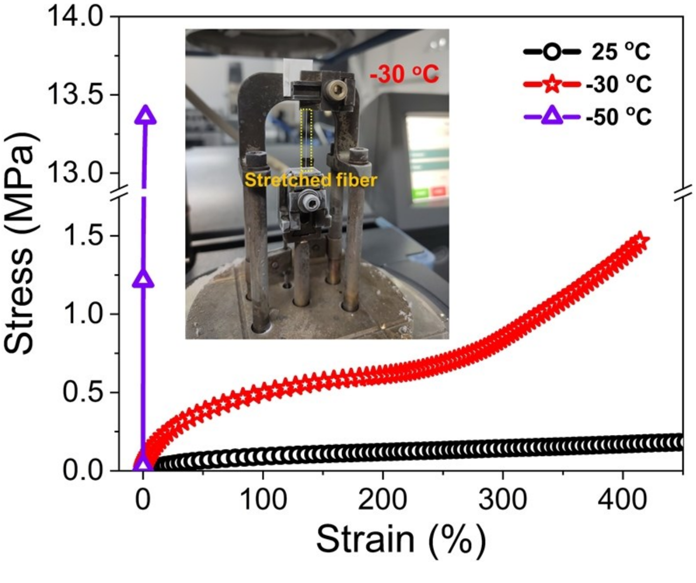

Fig. S3 DMA tensile curves of P(MEA-*co*-MTMA TFSI) ionogel fiber at different temperatures. The inset picture shows that the ionogel fiber remains elastic at −30 °C.

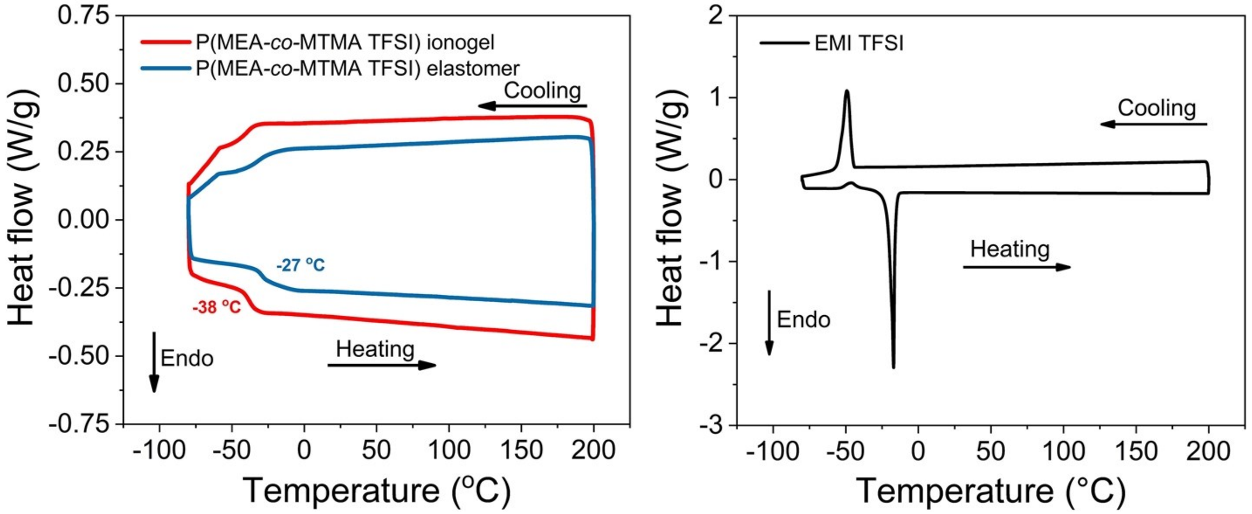

Fig. S4 DSC curves of P(MEA-*co*-MTMA TFSI) (ionogel and elastomer) and EMI TFSI. The glass transition temperature (T_g) of P(MEA-*co*-MTMA TFSI) ionogel (-38 °C) is lower than that of neat elastomer (without IL, -27 °C). The characteristic freezing peak of EMI TFSI was not observed in the ionogel, suggesting the good compatibility between IL and polymer.

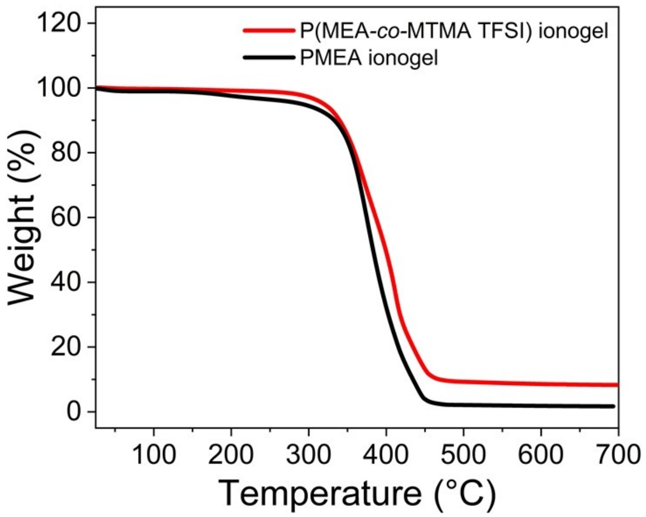

Fig. S5 TGA curves of P(MEA-*co*-MTMA TFSI) and PMEA ionogels. The decomposition temperatures were taken at 5 wt% mass loss. The decomposition temperature of P(MEA-*co*-MTMA TFSI) ionogel (320 °C) is higher than that of PMEA ionogel (280 °C).

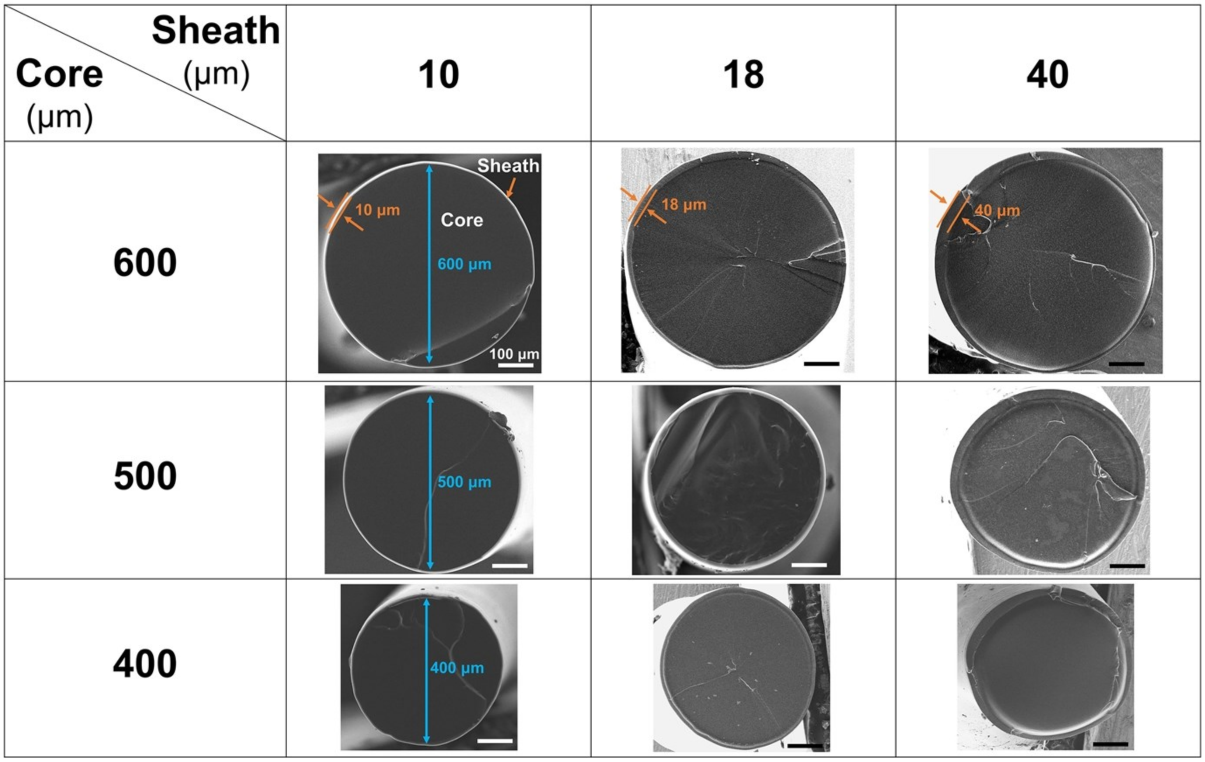

Fig. S6 Fractured SEM images of the smooth sheath-core fibers with varied core diameters and sheath thicknesses. The ionogel core diameter was controlled by the PTFE tube size, and the sheath thickness was controlled by the concentration of fluoroelastomer in MIBK.

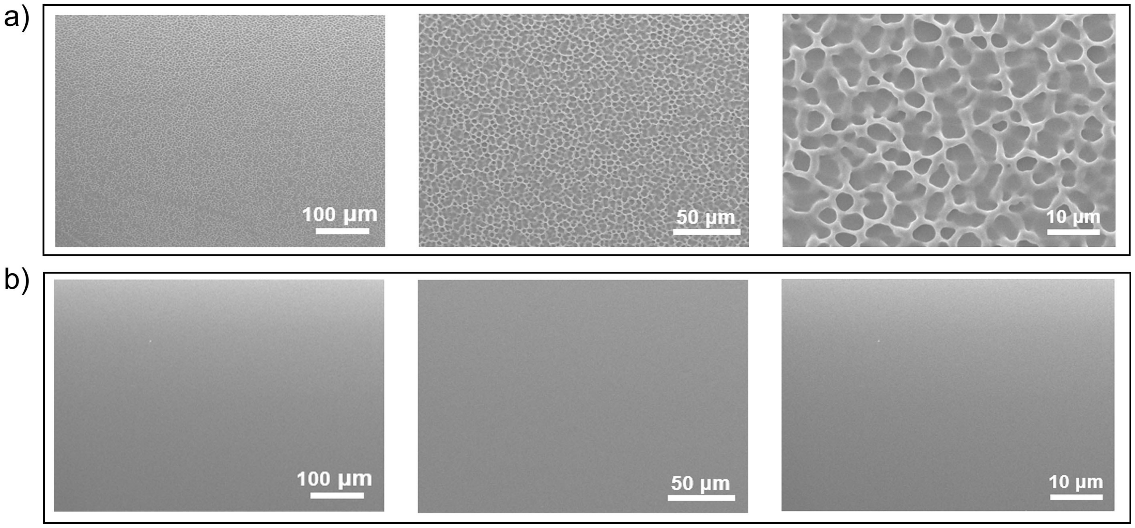

Fig. S7 SEM images of the sheath surfaces prepared at (a) high humidity (RH 90%) and (b) low humidity (RH 15%), respectively.

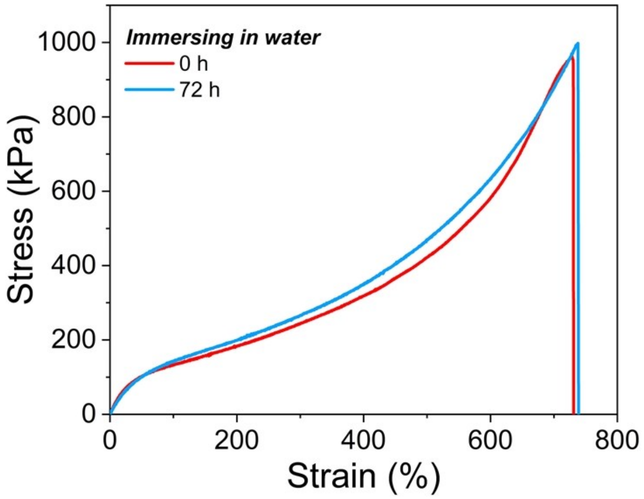

Fig. S8 Tensile stress-strain curves of the smooth sheath-core fiber before and after immersing in water for 72 h.

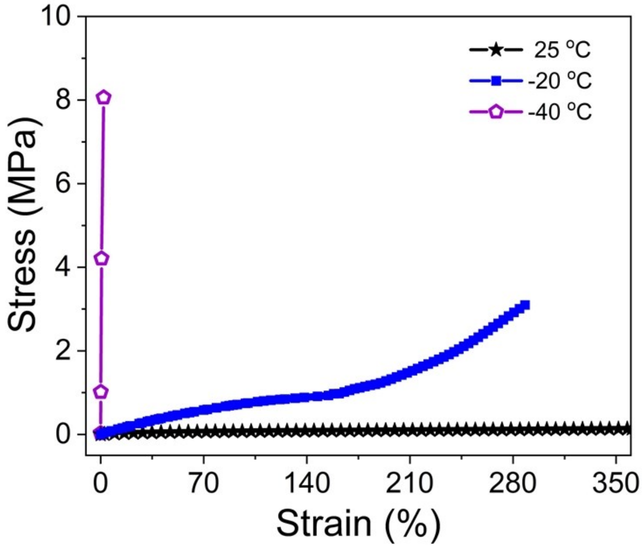

Fig. S9 DMA tensile curves of the smooth sheath-core fiber at different temperatures.

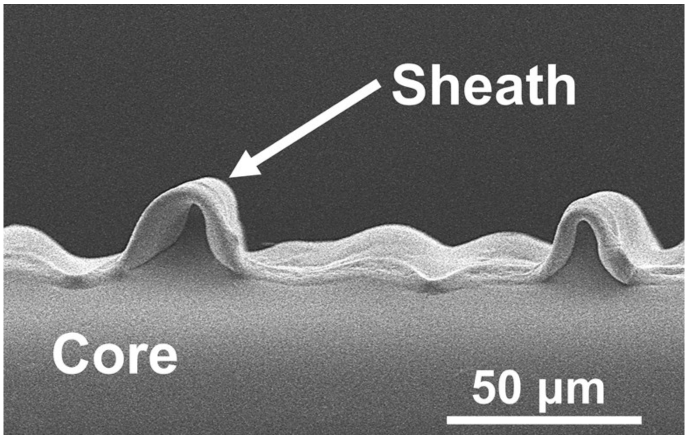

Fig. S10 Delamination occurs in the buckled sheath-core fiber without adding PEGDA in the sheath solution.

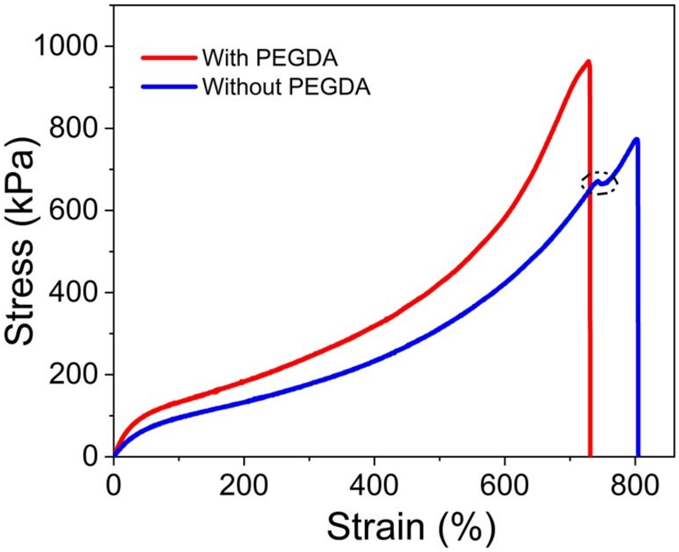

Fig. S11 Tensile curves of the sheath-core fibers with/without PEGDA. The dotted circle indicates the presence of a segmental fracturing point in delaminated sheath-core fiber.

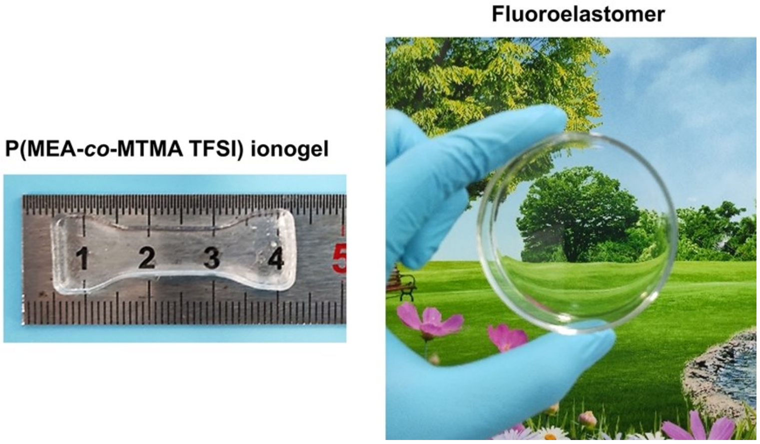

Fig. S12 Photos of P(MEA-*co*-MTMA TFSI) ionogel and PVDF-HFP-TFE fluoroelastomer film. The thicknesses of the two samples are 3 mm and 0.5 mm, respectively.

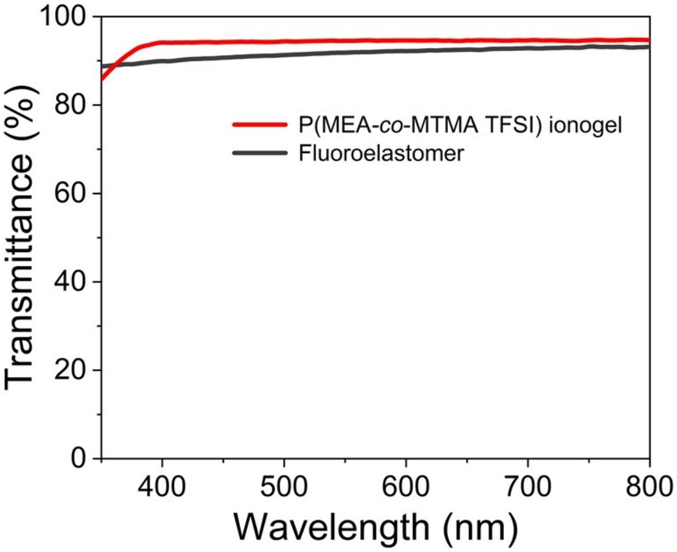

Fig. S13 UV-Vis transmittance spectra of P(MEA-*co*-MTMA TFSI) ionogel (1 mm thick) and fluoroelastomer (0.5 mm thick).

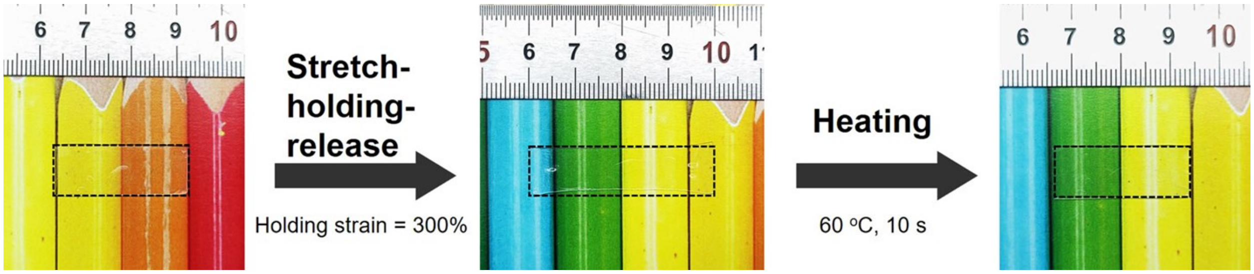

Fig. S14 Heat-induced full recovery of fluoroelastomer film formed by a stretch-holding-release process at 300% holding strain. The film has an initial length of 2.9 cm, and after stretching and holding for 5 min, became 4.1 cm long. Heating completely eliminated the residual strain with the film length recovering to 2.9 cm.

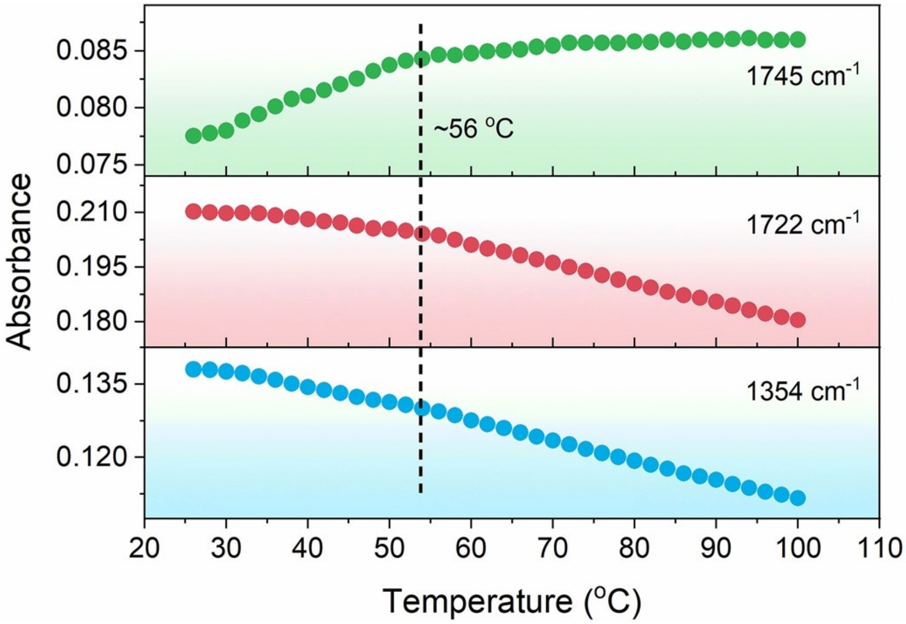

Fig. S15 Temperature-dependent spectral intensity variations of *v*(C=O) (free) around 1745 cm^{-1}, *v*(C=O) (dipolar coupling) around 1722 cm^{-1} and *v*(S=O) around 1354 cm^{-1}.

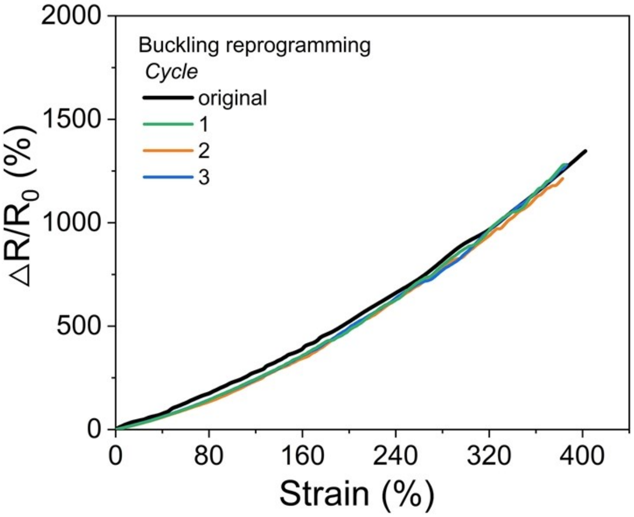

Fig. S16 Tensile strain-dependent resistance changes of the buckled sheath-core fiber through several reprogramming cycles (produced at 400% holding strain).

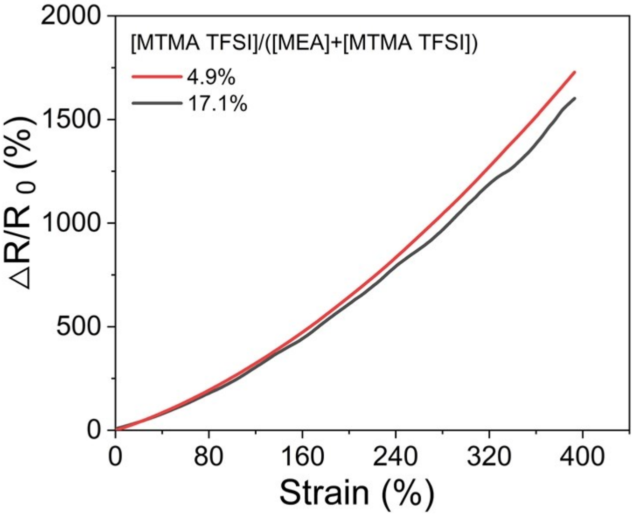

Fig. S17 Tensile strain-dependent resistance changes of buckled sheath-core fibers with different amounts of MTMA TFSI (i.e. different ionic conductivities). The two fibers were both produced at 500% holding strain. A higher ionic conductivity (4.9% MTMA TFSI) is helpful to improve the signal-to-noise ratio, but does not significantly influence the sensitivity.

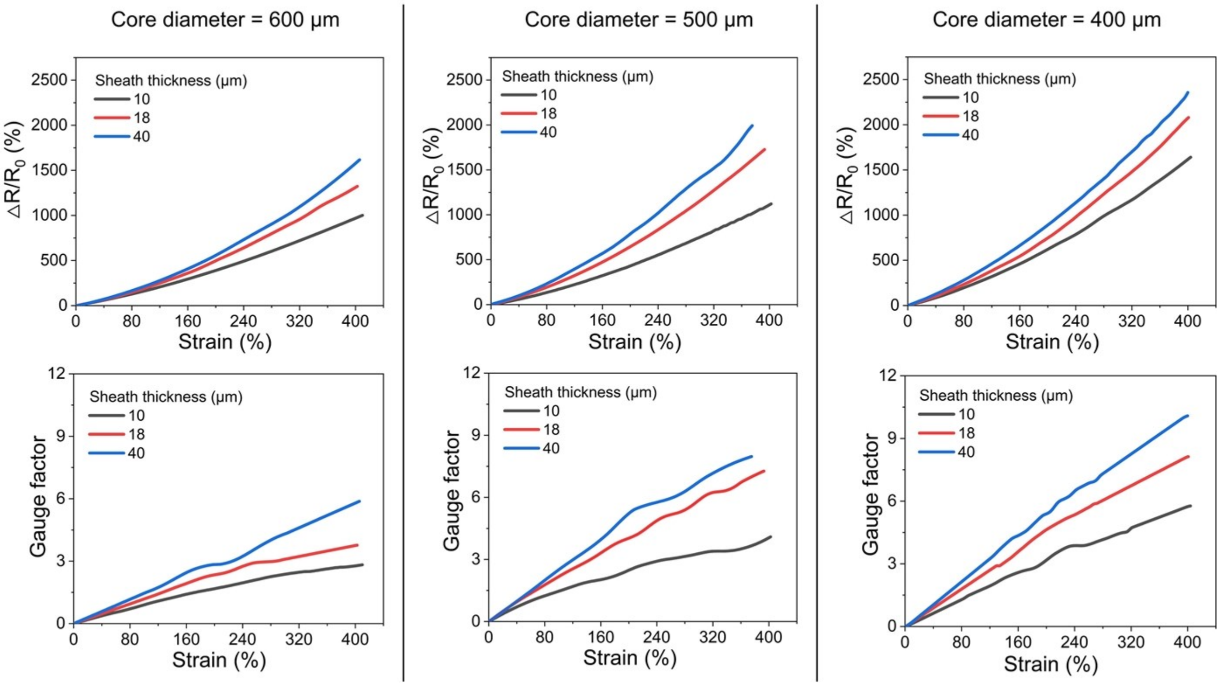

Fig. S18 Tensile strain-dependent resistance changes and corresponding gauge factors of buckled sheath-core fibers with different core diameters and sheath thicknesses. All the fibers were produced at 500% holding strain. The maximum gauge factors measured at 400% strain are listed in Table S2.

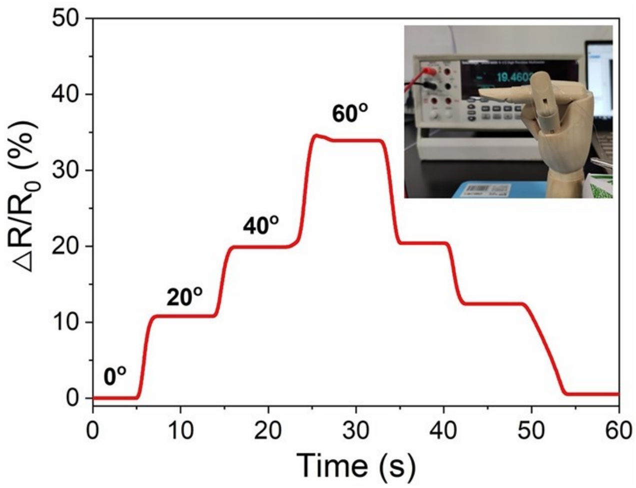

Fig. S19 Demonstration of prosthetic finger bending detected with buckled fiber strain sensor.

Table S1. Optimization of the ionogel precursor composition by varying MEA and MTMA TFSI concentrations. Entry 4 was selected as the optimal recipe.

Entry	Weight (g)					[MTMA TFSI] : ([MEA]+[MTMA TFSI])
	MEA	MTMA TFSI	EMI TFSI (0.64M)	PEGDA	DEAP	
1	1.012	0	0.3	0.0023	0.0016	0
2	1.012	0.0579 (0.1 M)	0.3108	0.0024	0.00165	1.6%
3	1.012	0.1204 (0.2 M)	0.3231	0.0024	0.00167	3.2%
4	1.012	0.1880 (0.3 M)	0.3365	0.00245	0.0017	4.9%
5	1.012	0.4290 (0.6 M)	0.3839	0.0026	0.0018	10.6%
6	1.012	0.7494 (0.9 M)	0.4470	0.0028	0.0020	17.1%

Table S2. Comparison of the maximum gauge factors of buckled sheath-core fibers with different core diameters and sheath thicknesses (original data in Fig. S18). The fiber in entry 5 is the representative sample studied in this work.

Entry	Core diameter (μm)	Sheath thickness (μm)	Gauge factor (at 400% strain)
1	600	10	2.9
2		18	3.8
3		40	5.9
4	500	10	4.1
5		18	7.3
6		40	8.0
7	400	10	5.8
8		18	8.1
9		40	10.1

Table S3. Comparison of the maximum strain and gauge factor of the buckled sheath-core fiber in this work with several other reported ionic sensors.

Ionic sensors	Max. strain (%)	Gauge factor (measured strain)	Ref.
Buckled sheath-core fiber	730	10.1 (400%)	This work
P(SPMA-r-MMA) hydrogel	2636	1.1 (200%)	S3
P(AAm-co-PAA)/Fe(III) hydrogel fiber	500	2 (120%)	S4
SA/NaCl/PAM hydrogel	2000	2.7 (1800%)	S5
PMMA-r-PBA ionogel	850	2.73 (100%)	S6
TA@HAP NWs-PVA hydrogel	480	2.84 (350%)	S7
PolyTA ionogel	2300	5.91 (2000%)	S8
LA-based ionic elastomer	1092	3.69 (300%)	S9
PVA-CNF organohydrogel	660	1.5 (400%)	S10
HPC/PVA hydrogel	800	2.8 (400%)	S11
PU-IL ionogel	327	1.54 (300%)	S12
PHEA/SA organohydrogel fiber	409	1.87 (200%)	S13
P(MEA-co-IBA) ICE	1640	6 (200%)	S14
PNA/PMA hydrogel fiber	900	0.94 (300%)	S15

References

S1 M. Tokuda, H. Minami, Y. Mizuta and T. Yamagami, *Macromol. Rapid Commun.*, 2012, **33**, 1130-1134.

S2 S. Morita, H. Shinzawa, I. Noda and Y. Ozaki, *Appl. Spectrosc.*, 2006, **60**, 398-406.

S3 J. Lee, M. W. M. Tan, K. Parida, G. Thangavel, S. A. Park, T. Park and P. S. Lee, *Adv. Mater.*, 2020, **32**, 1906679.

S4 M. Ju, B. Wu, S. Sun and P. Wu, *Adv. Funct. Mater.*, 2020, **30**, 1910387.

S5 X. Zhang, N. Sheng, L. Wang, Y. Tan, C. Liu, Y. Xia, Z. Nie and K. Sui, *Mater. Horiz.*, 2019, **6**, 326-333.

S6 Y. M. Kim and H. C. Moon, *Adv. Funct. Mater.*, 2020, **30**, 1907290.

S7 J. Wen, J. Tang, H. Ning, N. Hu, Y. Zhu, Y. Gong, C. Xu, Q. Zhao, X. Jiang, X. Hu, L. Lei, D. Wu and T. Huang, *Adv. Funct. Mater.*, 2021, **31**, 2011176.

S8 Y. Wang, S. Sun and P. Wu, *Adv. Funct. Mater.*, 2021, **31**, 2101494.

S9 C. Dang, M. Wang, J. Yu, Y. Chen, S. Zhou, X. Feng, D. Liu and H. Qi, *Adv. Funct. Mater.*, 2019, **29**, 1902467.

S10 Y. Ye, Y. Zhang, Y. Chen, X. Han and F. Jiang, *Adv. Funct. Mater.*, 2020, **30**, 2003430.

S11 Y. Zhou, C. Wan, Y. Yang, H. Yang, S. Wang, Z. Dai, K. Ji, H. Jiang, X. Chen and Y. Long, *Adv. Funct. Mater.*, 2019, **29**, 1806220.

S12 T. Li, Y. Wang, S. Li, X. Liu and J. Sun, *Adv. Mater.*, 2020, **32**, 2002706.

S13 J. Song, S. Chen, L. Sun, Y. Guo, L. Zhang, S. Wang, H. Xuan, Q. Guan and Z. You, *Adv. Mater.*, 2020, **32**, 1906994.

S14 B. Yiming, Y. Han, Z. Han, X. Zhang, Y. Li, W. Lian, M. Zhang, J. Yin, T. Sun, Z. Wu, T. Li, J. Fu, Z. Jia and S. Qu, *Adv. Mater.*, 2021, **33**, 2006111.

S15 L. Shuai, Z. H. Guo, P. Zhang, J. Wan, X. Pu and Z. L. Wang, *Nano Energy*, 2020, **78**, 105389.